Medical Engineering & Physics 32 (2010) 957–967

Contents lists available at ScienceDirect

Medical Engineering & Physics

journal homepage: www.elsevier.com/locate/medengphy

Estimation of distributed arterial mechanical properties using a wave propagation model in a reverse way

C.A.D. Leguy [a,*], E.M.H. Bosboom [b], H. Gelderblom [a], A.P.G. Hoeks [b], F.N. van de Vosse [a]

[a] Department of Biomedical Engineering, Eindhoven University of Technology, Eindhoven, The Netherlands
[b] Department of Biomedical Engineering, Maastricht University Medical Center, Maastricht, The Netherlands

ARTICLE INFO

Article history:
Received 23 September 2009
Received in revised form 12 February 2010
Accepted 27 June 2010

Keywords:
Arterial stiffness
Young's modulus
Brachial artery
Wave propagation model
Ultrasound
Sensitivity analysis

ABSTRACT

To estimate arterial stiffness, different methods based either on distensibility, pulse wave velocity or a pressure-velocity loop, have been proposed. These methods can be employed to determine the arterial mechanical properties either locally or globally, e.g. averaged over an entire arterial segment. The aim of this study was to investigate the feasibility of a new method that estimates distributed arterial mechanical properties non-invasively. This new method is based on a wave propagation model and several independent ultrasound and pressure measurements. Model parameters (including arterial mechanical properties) are obtained from a reverse method in which differences between modeling results and measurements are minimized using a fitting procedure based on local sensitivity indices. This study evaluates the differences between in vivo measured and simulated blood pressure and volume flow waveforms at the brachial, radial and ulnar arteries of 6 volunteers. The estimated arterial Young's modulus range from 1.0 to 6.0 MPa with an average of (3.8 ± 1.7) MPa at the brachial artery and from 1.2 to 7.8 MPa with an average of (4.8 ± 2.2) MPa at the radial artery. A good match between measured and simulated waveforms and the realistic stiffness parameters indicate a good in vivo suitability.

1. Introduction

Arterial stiffness, S, is an independent predictor of cardiovascular risk at an early stage [1] and is increasingly assessed in clinical practice [2–6].

To study the relations between arterial properties such as arterial stiffness and parameters such as blood pressure and blood volume flow (BVF), lumped parameter [7–11] or one-dimensional wave propagation models [12–16] can be used. The wave propagation models are based on governing equations (conservation of mass and momentum) and constitutive equations that describe the mechanical properties of the arterial wall. Wave propagation models are adapted to simulate wave propagation phenomena while demanding only few minutes of calculation time. Experimental and clinical validation models have been performed and demonstrated the ability to qualitatively describe blood pressure and blood volume flow waveforms [15,17,18]. Furthermore, wave propagation models were successfully employed to simulate the effects of (surgical) interventions [19] or predict the effect of pathophysiological conditions.

Wave propagation models cannot be used to estimate arterial stiffness directly, since arterial diameters, wall thicknesses and arterial wall mechanical properties like the Young's modulus are required as input. However, the model output, expressed in the BVF and blood pressure waveforms, can be employed to estimate arterial mechanical properties in a reverse process comparing model output with the corresponding measurements. Input parameters (including the arterial mechanical properties) are optimized until the best fit between measured and simulated BVF and blood pressure waveforms is obtained.

For the measurements required for such reverse method, ultrasound is the favorable imaging tool. Both perpendicular echo M-mode and oblique Doppler measurements can be performed with a high temporal resolution, to determine the vessel wall distension waveform and centerline blood velocity, respectively [20]. Then, scaling of the measured distension waveform with the systolic and diastolic blood pressure can be performed to approximate the blood pressure waveform. Furthermore, BVF can be obtained from the centerline velocity using Womersley profiles [20].

An initial estimate of the arterial stiffness is also required. Several methods have been proposed to estimate arterial stiffness non-invasively. Most commonly, the arterial stiffness is assessed locally from the time average vessel radius, $\bar{a}$, and the linearized vessel wall distensibility, D_0. The distensibility D_0 is defined as the ratio between the linearized compliance C_0 and the time average

* Corresponding author at: Department of Biomedical Engineering, Eindhoven University of Technology, PO Box 513, WH 4.33, 5600 MB Eindhoven, The Netherlands. Tel.: +31 40 247 40 60; fax: +31 40 244 7355.
E-mail address: leguycarole@gmail.com (C.A.D. Leguy).

1350-4533/$ – see front matter © 2010 IPEM. Published by Elsevier Ltd. All rights reserved.
doi:10.1016/j.medengphy.2010.06.010

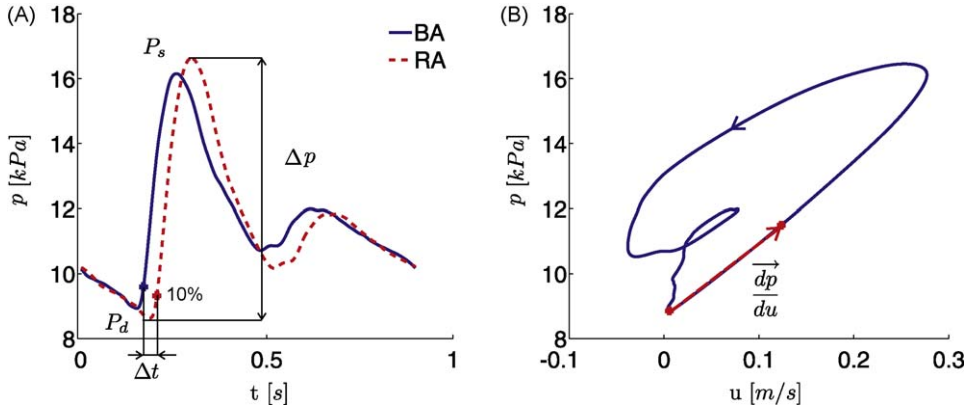

Fig. 1. (A) PWV method: the 10% foot (time when the pressure reaches 10% of Δp) during the systole is depicted. (B) The PU-loop method: the derivative of the pressure with respect to the average blood velocity is shown during the linear part of the systolic phase.

cross-sectional area $\bar{A}$:

$$D_0 = \frac{1}{\bar{A}}\frac{\Delta A}{\Delta p} = \frac{C_0}{A}, \quad \text{with} \quad C_0 = \frac{\Delta A}{\Delta p}, \tag{1}$$

ΔA being the maximum area difference and Δp the corresponding pressure difference within a heart cycle.

If we assume a linear elastic and isotropic behaviour, arterial stiffness S can be defined as the product between the Young's modulus, E, and the time average vessel wall thickness, $\bar{h}$, and can be calculated from the following relation [11]:

$$S = E\bar{h} = \frac{2[(2\bar{a}^2(1-\mu^2))/\bar{h} + (1+\mu)(2\bar{a}+\bar{h})]}{D_0((2\bar{a}/\bar{h})+1)}, \tag{2}$$

Herein μ is the Poisson ratio. When the wall thickness, $\bar{h}$, is an order of magnitude smaller than the radius $\bar{a}$, the following thin-walled tube formulation is obtained:

$$S \approx \frac{2\bar{a}(1-\mu^2)}{D_0}. \tag{3}$$

This relation is usually applied to common carotid, femoral or brachial arteries to derive a local arterial stiffness [4,21,22]. For all these arteries, the local pulse pressure is assumed to equal the brachial pulse pressure Δp. The radius $\bar{a}$ and ΔA can be assessed using an ultrasound scanner.

For arteries that are not accessible by ultrasound, an alternative method based on the global pulse wave velocity, c_0, can be employed. In the so-called pulse wave velocity (PWV) method, pressure waveforms obtained with applanation tonometry, or wall distension waveforms obtained with ultrasound techniques, are measured at a proximal and a distal site. For both waveforms, the foot of the wave is defined as the time when the pressure reaches 10% of its pulse Δp (see Fig. 1A). Alternatively for the common carotid artery the dicrotic notch can be chosen as reference point [23]. The distance between the measurement sites, Δl, is divided by the foot-to-foot or dicrotic notch transit time, Δt, to calculate the pulse wave velocity c_0. The distensibility D_0, is then estimated with the Moens-Korteweg wave speed c_0 for thin-walled tube assuming that the vessel wall behaves linear elastically, isotropically and incompressibly:

$$D_0 \approx \frac{1}{\rho c_0^2}, \quad \text{with} \quad c_0 = \frac{\Delta l}{\Delta t}, \tag{4}$$

with ρ the blood density. Next, either (2) or (3) can be used to estimate an average S over the arterial segment. Most commonly, the PWV is estimated between the carotid and femoral arteries, or between the brachial and radial arteries.

An alternative method, developed by Parker and Jones [24], is based on the pressure-velocity-loop (PU-loop) and requires the simultaneous assessment of the mean blood flow velocity over the arterial cross-section, u, and blood pressure, p. It is assumed that no reflections are present during the early systole and that the relation between p and u is linear (see Fig. 1B). The PWV, c_0, is then estimated from the slope of the PU-loop, with:

$$c_0 = \frac{1}{\rho}\frac{dp}{du}. \tag{5}$$

Since it is not possible to assess the blood pressure waveform non-invasively, p is approximated by the vessel wall distension waveform scaled with the systolic and diastolic blood pressures assuming a linear pressure–area relationship [25]. The scaling will not affect the temporal relationships.

Arterial stiffness can be estimated globally with the PWV method or locally using either the distensibility or the PU-loop method. All these methods have some drawbacks. The distensibility method reflects the arterial mechanical properties at a single location. Furthermore, it requires local pulse pressure while it can only be measured directly in the brachial artery. The PWV method estimates an average stiffness over a long arterial trajectory whereas stiffness differs between arteries and increases towards the peripheries [26]. Finally, for both PWV and PU-loop methods, hemodynamic viscous forces and pressure wave reflections originating from transitions in arterial stiffness, the presence of bifurcations, arterial lumen tapering and the peripheral bed are neglected. These assumptions might lead to inaccuracies in the estimates of arterial stiffness.

The aim of the present study is to investigate the feasibility of a non-invasive method to estimate distributed arterial mechanical properties by means of a reverse approach of a 1D wave propagation model, as developed by Bessems et al. [13], in combination with several independent ultrasound and blood pressure measurements.

An estimate of the distributed arterial properties along each arterial segment is obtained whereas other techniques are providing either local or average estimates. Furthermore, several independent ultrasound measurements are combined, which might reduce the sensitivity of the method to measurement errors. Moreover, this approach is based on a model taking into account hemodynamic viscous forces, pressure wave propagation and reflection phenomena.

We focus on the estimation of the mechanical properties of the arteries of arm because these arteries are frequently subject of medical investigations [27–29]. Furthermore, the local systolic and diastolic blood pressure can be measured directly in the brachial artery and ultrasound measurements can be performed in the main arteries from the arm pit until the wrist, enabling the estimation of vessel wall distension and BVF at several sites.

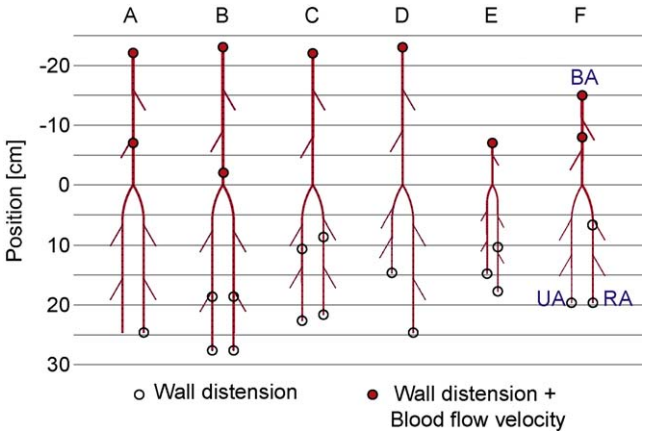

Fig. 2. Arterial tree model geometry for the 6 volunteers, and wall distension and blood flow velocity measurements locations in the brachial (BA), radial (RA) and ulnar artery (UA). The labels A, B, C, D, E and F correspond to the 6 subjects.

In this study, we decided to concentrate on the estimation of the Young's modulus E since the wall thickness $\bar{h}$ is too small to be measured directly and will be estimated from the diameter measurement assuming proportionality. The arterial stiffness, S, can be derived by multiplying E by $\bar{h}$.

In the first part of this paper, the protocol for the in vivo ultrasound measurements is presented. Then the wave propagation model and the fitting procedure based on the local sensitivity index are described. Subsequently, the parameter estimates resulting from this fitting procedure are shown and discussed.

2. Materials and methods

2.1. In vivo measurements

2.1.1. Measurement protocol

This study involved a group of six healthy and non-smoking young male volunteers. Their average age was 25 years (range 21–34), their average weight 83 kg (range 74–95 kg) and their average height 1.89 m (range 1.75–2.02 m). All subjects had given written informed consent. The study was approved by the joint Medical Ethical Committee of the University Maastricht and the University Hospital Maastricht.

A set of local ultrasound measurements was obtained to provide vessel wall distension and BVF velocity. These measurements were performed in the left arm, if possible distal and proximal in the brachial, ulnar and radial artery; see Fig. 2. The location of the bifurcation of the brachial to radial and ulnar arteries was identified in echo B-mode. The ultrasound measurements were performed at least 2 cm from the bifurcation, with the arm in a slightly bent position. The distance of the measurement location to the bifurcation was measured on the body surface using a tape measure.

The measurements started after 10 min rest in supine position to allow normalization of cardiovascular function. Each measurement covered 4 consecutive heart beats and was repeated at least three times. The measurement session lasted at most two hours. Brachial systolic P_s and diastolic P_d blood pressures were measured non-invasively with a semi-automated oscillometric device (Dynamap, Critikon, Tampa, USA) at the start and end of the measurement session.

2.1.2. Wall distension and blood volume flow estimations

The ultrasound measurements were performed using an ultrasound system (Ultramark 9 plus, Advanced Technology Laboratories, Bellevue, WA, USA) equipped with a linear array probe (7.5 MHz) set in M-mode for wall distension assessment, and with a curved-array transducer (5–9 MHz) activated in a wide-band M-mode with a high pulse-repetition frequency of 10 kHz for blood velocity assessment [30].

The distension waveform was obtained off-line with a proprietary radio-frequency acquisition system [31]. To obtain blood flow velocities, a cross-correlation function was applied to short radio-frequency data segments [32]. Each velocity estimate is based on half overlapping data segments corresponding to 300 mm in depth and 10 ms in time. In this way, instantaneous time dependent velocity profiles along a single line of observation are obtained.

The blood flow velocity could only be successfully measured in the brachial artery (BA). Similar measurements were attempted in the radial artery (RA) and ulnar artery (UA). Because of the small size of these arteries and their very superficial location, the quality of the velocity estimates was not sufficient to be included in this study.

Because of important spatial limitations due to ultrasound reflections close to the interface between the lumen and the vessel wall [33,34], simple integration of the acquired velocity profile is not feasible. Thus, blood volume flow, q, in the BA was estimated from the centerline velocity using the Womersley profile method [20,35] and a time average radius $\bar{a}$ from the distension waveform.

2.1.3. Measurement variability

To quantify the repeatability of the measurements, the variability of the measured parameters was investigated. The intra- and inter-subject variability, σ_m and σ_g, were obtained.

The intra-subject variability σ_m, that evaluates the variability between the measurements in each volunteer, is expressed as:

$$\sigma_m = \sqrt{\frac{\sum_v \sum_m (X_{v,m} - \bar{X}_v)^2}{\sum_v (M_v - 1)}}, \tag{6}$$

with $X_{v,m}$ the value for volunteer v of measurement m and $\bar{X}_v$ the average for each volunteer v. The number of measurements for the volunteer v is represented by M_v.

The variability between the different volunteers of the group was evaluated by the inter-subject variability σ_g, which is defined as

$$\sigma_g = \sqrt{\frac{\sum_v (\bar{X}_v - \bar{X})^2}{N - 1}}, \tag{7}$$

$\bar{X}$ being the average of the group, and N the number of volunteers.

2.1.4. Estimation of arterial stiffness using distensibility, PWV and PU-loop methods

Distensibility, PWV, and PU-loop methods were employed to obtain an initial estimate for E, using (2). The distensibility method was applied to the wall distension measurements performed in the BA, where the local pulse pressure follows from the difference between the measured P_s and P_d and ΔA from the distension waveform. The PWV method was applied to the distension waveforms measured in the BA and RA using the foot-to-foot transit time. Finally, the PU-loop method was applied to the wall distension and BVF measurements in the BA.

2.2. The wave propagation model

The wave propagation model used in this paper has been developed by Bessems et al. [13], and is validated experimentally in a subsequent study [18]. The conservation of mass and momentum equations were solved considering blood as a Newtonian fluid. A velocity profile was introduced based on boundary layer theory.

The governing equations were solved applying a spectral element method.

The arterial wall was modeled as a thick-walled linear elastic material according to (2) and arteries were terminated by a 3-element Windkessel model [36].

2.3. Initial model parameterisation

To be able to develop an efficient reverse method, it is necessary to use as few characteristic input parameters as possible. Therefore rules are formulated to minimize the number of parameters defining geometry, boundary conditions, and mechanical behavior of the modeled arterial system.

2.3.1. Model geometry

The three main arteries of the arm were represented by the BA bifurcating into the RA and UA, see Fig. 2. Six extra side branches, having a length of 4 cm, were added to model the arterial network of smaller sized arteries like the superior and inferior ulnar, the radial recurrent and the dorsal interosseous arteries. These side branches supply blood volume to the surrounding tissue (muscles of the arm) and contribute to the distribution of BVF along the upper limb model. Each arterial segment was divided into elements with a length of 1 cm (sufficiently small to ensure numerical convergence), whereas a bifurcation element ensured continuity of pressure and flow, see Fig. 2.

The measured vessel radius is used to build a patient specific mesh, but since the measurement locations are sparse, an interpolation is used for the radii of the entire arterial tree. The vessel radius is assumed to decrease exponentially along the arterial tree. The vessel radius $\bar{a}$ at a position z along the artery is then defined as

$$\bar{a}(z) = \bar{a}_{z_0} \ \exp(-\alpha_{\bar{a}} z), \tag{8}$$

with $\bar{a}_{z_0}$ the radius at $z = 0$, and $\alpha_{\bar{a}}$ the tapering factor. This definition holds for an arterial segment without bifurcation [10,26,37].

To define diameters at bifurcations, the time average wall shear stress, $\bar{\tau}$, along the arterial tree was assumed to be constant. Then, according to Murray's law, the third power of the mother artery radius, a_m, equals the sum of the third power of the two daughter artery radii, a_{d_1} and a_{d_2} [38,39]:

$$a_m^3 = a_{d_1}^3 + a_{d_2}^3. \tag{9}$$

Eqs. (8) and (9) are applied to the BA, RA and UA. The obtained system of 4 equations with 4 unknowns is then solved to determine the tapering factor $\alpha_{\bar{a}}$.

For the side branches, as it was not possible to assess the radius of these small vessels using ultrasound, an estimate of the radius has been obtained. Assuming a Womersley velocity profile and non-moving walls, $\bar{\tau}$ is defined as

$$\bar{\tau} = \frac{4\eta\bar{q}}{\pi\bar{a}^3}, \tag{10}$$

with $\bar{q}$ the time average BVF and η the blood viscosity chosen equal to 4×10^{-3} Pa s [40]. Applying the two radius measurements in the BA, we could determine that the blood flow should decrease by 30% along the BA. Considering two side branches in the BA, and $\bar{\tau}$ constant, the following relation could then be used:

$$a_s^3 = 0.15 a_m^3, \tag{11}$$

with a_s and a_m the radius of the side branch and the mother artery, respectively.

2.3.2. Arterial wall properties

Since arterial stiffness increases toward the peripheries, an exponential model is used to describe the Young's modulus, E, that can be expressed as

$$E(z) = E_0 \ \exp(-\alpha_E z), \tag{12}$$

with E_0 the proximal Young's modulus and α_E a stiffening factor [26,37].

The arterial wall thickness, $\bar{h}$, could not be estimated accurately from the measurements, thus a standard ratio between $\bar{h}$ and the mean radius $\bar{a}$ of 15% has been used for the BA, and 20% for the RA and UA [41–43]. The wall thickness is thus not fitted together with the other parameters, but explicitly chosen. As Eh is the arterial stiffness, this could influence the estimations of the Young's modulus.

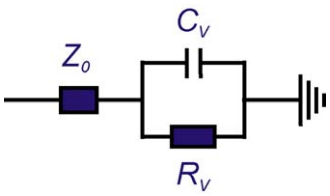

Fig. 3. End-segment 3-element Windkessel model composed of a characteristic impedance Z_0, an end-resistance R_v and a compliance C_v.

2.3.3. Boundary conditions

The BVF obtained proximal in the BA was defined as the entrance flow, q_i, and used as an input for the simulations.

The RA, UA and small side branches were terminated with a 3-element Windkessel model composed of a characteristic impedance Z_0, an end-resistance R_v and a compliance C_v (Fig. 3). The peripheral resistance, R, can be expressed as function of the peripheral resistances R_j at each extremity such that

$$\frac{1}{R} = \sum_{j=1}^{n} \frac{1}{R_j}, \quad \text{with } R_j = R_{v_j} + Z_{0_j}. \tag{13}$$

Herein, R_{v_j} is the end-resistance, Z_{0_j} the characteristic impedance at each extremity j and n the number of end-segment.

Time constant τ_C is defined as $\tau_C = R_v C_v$ and is initially set to 1.5 s. A first approximation $\tilde{Z}_{0_j}$ of the characteristic impedance at each extremity j is obtained by assuming minimal reflection of high frequencies from the peripheries

$$\tilde{Z}_{0_j} = \sqrt{\frac{L_0}{C_0}} = \sqrt{\frac{\rho h E_j}{2\pi^2(1-\mu^2)\bar{a}_j^5}}, \tag{14}$$

with $L_0 = \rho/(\pi\bar{a}_j^2)$ being the local inertance, C_0 the local compliance assuming a thin-walled tube, $\bar{a}_j$ the vessel radius and E the Young's modulus. A factor K_{Z_0}, initially set to 1, is then used to modify the first approximation $\tilde{Z}_{0_j}$ of Z_{0_j} such that

$$Z_{0_j} = K_{Z_0} \tilde{Z}_{0_j}. \tag{15}$$

The total peripheral resistance R is defined as the ratio between the time average pressure $\bar{p}$ and the BVF time average $\bar{q}$ such that

$$R = \frac{\bar{p}}{\bar{q}}. \tag{16}$$

The time average pressure $\bar{p}$ is estimated from the wall distension waveform at the BA, scaled with P_s and P_d to obtain a blood pressure waveform [25]. Since the time average wall shear stress is assumed to be equal for all the extremities, the total resistance at extremity j, R_j, is for a time averaged Poiseuille profile inversely proportional

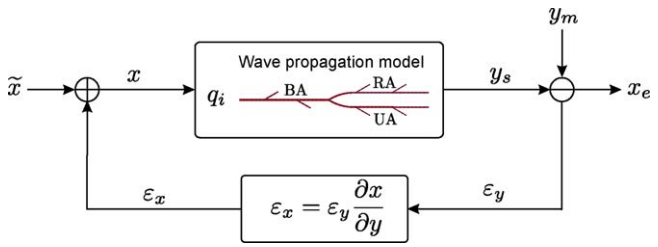

Fig. 4. The reverse method fitting scheme with $\tilde{x}$, x, x_e, the initial, current and final estimates of the input parameters, respectively; y_s and y_m are the simulated and measured output parameters; q_i is the input blood volume flow; ε_y is the current error in output parameters and ε_x is the correction value for the input parameters.

to the third power of the radius $\bar{a}_j$:

$$R_j = \frac{\bar{p}}{\bar{q}} \frac{\sum a_{0_j}^3}{a_{0_j}^3}. \tag{17}$$

2.4. The reverse approach

The fitting process, as described in the following section, is based on the total end-resistance R, the proximal Young's modulus E_0, the stiffening factor α_E, the time constant τ_c, and the characteristic impedance factor K_{Z_0}. It is assumed that the vessel length and radii are measured accurately. Therefore the length, radii and the wall thickness, defined as a function of the radii, are fixed and not modified during the fitting procedure.

2.4.1. Local sensitivity analysis

A local sensitivity analysis has been performed to estimate the rate of change in the model output with respect to changes in the model input. The influence of the input parameters, R, E_0, α_E, τ_C and K_{Z_0} was investigated for the following output parameters that reflect the main characteristics of the pressure waveforms:

- the time average pressure $\bar{p}$;
- the pulse pressure Δp at the BA;
- the time derivative of the blood pressure during the systolic time period $\dot{p}$ (the time interval during which the pressure increased from 10% to 90% is used to calculate $\dot{p}$, see Fig. 1);
- the compliance C_0 at the BA;
- the transit time from the BA to RA and BA to UA: Δt_r and Δt_u;
- the distension ΔA_r and ΔA_u at the RA and UA, respectively.

The sensitivity of each parameter is evaluated by the relative sensitivity index $I_{i,k}$ of output parameter y_k to input parameter x_i, and is defined as

$$I_{i,k} = \frac{\partial y_k}{\partial x_i} \frac{x_i}{y_k}, \tag{18}$$

with

$$\frac{\partial y_k}{\partial x_i} = \frac{y(x_1, \ldots, x_{i-1}, x_i + \Delta x_i, x_{i+1}, \ldots, x_k) - y(x)}{\Delta x_i}. \tag{19}$$

2.4.2. Fitting process

Based on the sensitivity indices, simple fitting rules are applied to determine the input parameter set yielding the best fit between the measured and simulated data. A reversed method is used to iteratively minimize the difference between measured y_m and simulated y_s output parameters by optimizing the input parameter x_i, see Fig. 4. For the input x and the output y, the correction value for the input parameter, ε_x (in %), is estimated from the error in output parameters ε_y (in %) and the sensitivity index I (Eq. (18)):

$$\varepsilon_x = \frac{\varepsilon_y}{I}. \tag{20}$$

The results from the local derivative are used to predict the behavior of the model and thus to define the fitting steps. Those output variables that only depend on one input parameter are fitted first. The procedure is repeated until adjusting parameters no longer results in better fits.

The input parameters R, E_0, α_E, τ_c and K_{Z_0} are optimized. The estimates of E_0 obtained from the reverse method are compared to the ones determined by the distensibility, PWV, and PU-loop methods.

Table 1
Group average, inter-subject variability σ_g and intra-subject variability σ_m of the arterial radius ($\bar{a}$), the distension (Δa), the time average blood volume flow ($\bar{q}$) and the maximum blood volume flow (Q) for the 6 volunteers. The indices b, r, and u refer to the BA, RA and UA.

	Group average	σ_g	σ_m
P_s [mmHg]	119	±14	±4
P_d [mmHg]	67	±8	±5
$\bar{a}_b$ [mm]	2.3	±0.3	±0.1
$\bar{a}_r$ [mm]	1.2	±0.3	±0.2
$\bar{a}_u$ [mm]	1.1	±0.3	±0.1
Δa_b [%]	2.1	±1.6	±0.5
Δa_r [%]	1.2	±0.5	±0.5
Δa_u [%]	1.5	±0.7	±0.4
$\bar{q}$ [ml/min]	41	±26	±10
Q [ml/min]	288	±116	±42

3. Results

3.1. In vivo measurements

The systolic and diastolic blood pressure of the BA, radius and wall distension (defined as the percentage increase in radius within an heart cycle) of the BA, RA and UA, as well as the mean and maximum BVF measured in the BA are displayed in Table 1. The group average P_s and P_d equal (119 ± 14) and (67 ± 8) mmHg, with an intra-subject variability σ_m of 4 and 5 mmHg, respectively. The group average radii equal (2.3 ± 0.3) and (1.2 ± 0.3) mm, with a group average relative distension of (2.1 ± 1.6)% and (1.2 ± 0.5)% for the BA and RA, respectively. The inter- and intra-subject variabilities are small for the radius measurements but relatively large for the distension measurements. The time average BVF and maximum BVF in the BA are (41 ± 26) and (288 ± 116) ml/min with an intra-subject variability of 10 and 42 ml/min, respectively.

3.2. Initial parameter estimates

The Young's modulus is estimated using the distensibility (2), PWV (4) and PU-loop methods (5). As can be seen in Fig. 5, the estimates exhibit a wide variation due to measurement errors whereas differences between the estimates are large. Since, the PU-loop method results in non-physiological estimates for the Young's modulus (up to 35 MPa), we used the average of the estimates derived with the distensibility and the PWV methods as initial guess for the Young's modulus. The variation in the Young's modulus is in the order of 20% when the thin-walled tube approximation (3) is used instead of thick walled one (2).

The measured parameters used for the fitting process exhibit large uncertainties, see Table 2.

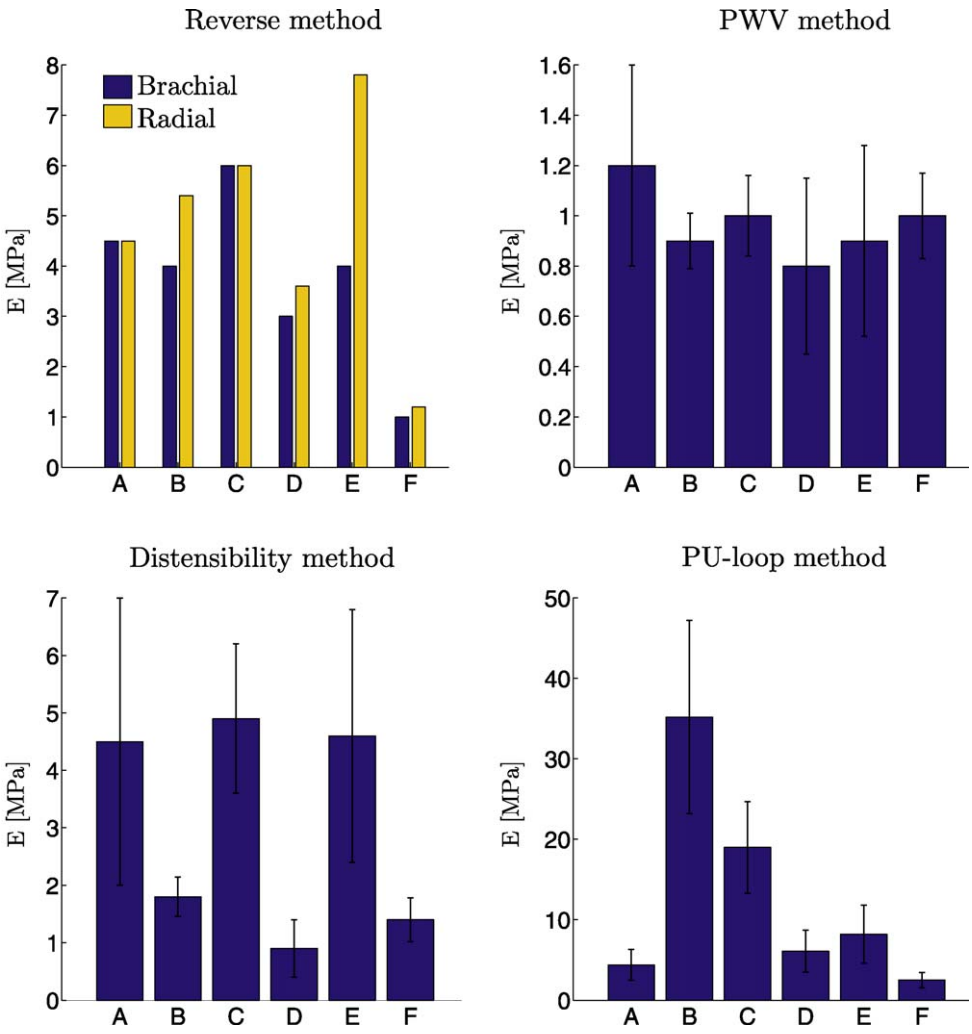

Fig. 5. Young's modulus estimates obtained for the brachial and radial arteries with the reverse method, the PWV, the distensibility and the PU-loop methods as well as the corresponding measurement uncertainties for the PWV, distensibility and PU-loop methods. The estimates are shown for the 6 volunteers, labeled with the letters A, B, C, D, E and F. Note the differences in vertical scaling.

3.3. Sensitivity analysis

The sensitivity indices obtained from the sensitivity analysis are presented in Fig. 6. Each index represents the percentage increase of the output parameter for a % increase in the input parameter. To enable an easier interpretation of the effect of the stiffening factor α_E, a 1% increase of the Young's modulus at the RA, E_r, is considered. Since the results for ΔA_u and Δt_u are similar to the results for ΔA_r and Δt_r, respectively, they are not included in the figure.

From the local sensitivity study, it follows that $\bar{p}$ only depends on R. The compliance C_0 is regulated solely by E_0. Thus, both $\bar{p}$ and C_0 can easily be set to the measured value by fixing R and E_0, respectively.

Table 2
Uncertainty in % of the measured time average pressure $\bar{p}$, pulse pressure Δp, pressure time derivative $\dot{p}$, compliance C_0, transit time Δt and distension ΔA for the 6 volunteers (A–F). The indices r and u refer to the RA and UA.

	$\bar{p}$	Δp	$\dot{p}$	C_0	Δt_r	Δt_u	ΔA_r	ΔA_u
A	±27%	±14%	±28%	±31%	±16%	×	±18%	×
B	±30%	±3.6%	±15%	±16%	±2%	±6%	±39%	±54%
C	±22%	±11%	±17%	±21%	±4%	±7%	±5%	±33%
D	±37%	±16%	±30%	±43%	±18%	±9%	±100%	±27%
E	±29%	±18%	±34%	±35%	±13%	±14%	±22%	±39%
F	±20%	±19%	±24%	±24%	±3%	±4%	±62%	±7%

The pulse pressure ΔP, is influenced by R, E_0, τ_C and K_{Z_0}. Because we do not want to modify E_0 and R, since they have been already used to set $\bar{p}$ and C_0, only τ_C and K_{Z_0} will be used to fit Δp. Subsequently, the stiffening factor α_E is used to fit ΔA_r and ΔA_u.

Following these four rules, all five input parameters have been used once in the fitting process. When the estimates obtained are not corresponding to the best fit between measured and simulated parameters, the two other output parameters Δt_r and $\dot{p}$ can be used to refine the estimate of K_{Z_0} and E_0 and obtain an optimized fit.

The fitting strategy is summarized by the following steps:

1. $\bar{p}$ is set by fixing R.
2. C_0 is set with E_0.
3. Δp is fitted by controlling τ_t and Z_0.
4. ΔA_r and ΔA_u are regulated with α_E.
5. Δt_r and Δt_u are set with Z_0 and E_0.
6. $\dot{p}$ is fitted with modifying E_0.

Using these basic rules, the differences between the measured and simulated data parameters are minimized to determine the patient specific model parameters for each of the volunteer. For each volunteer, around 20 iterations of the model were needed to obtain the best fit.

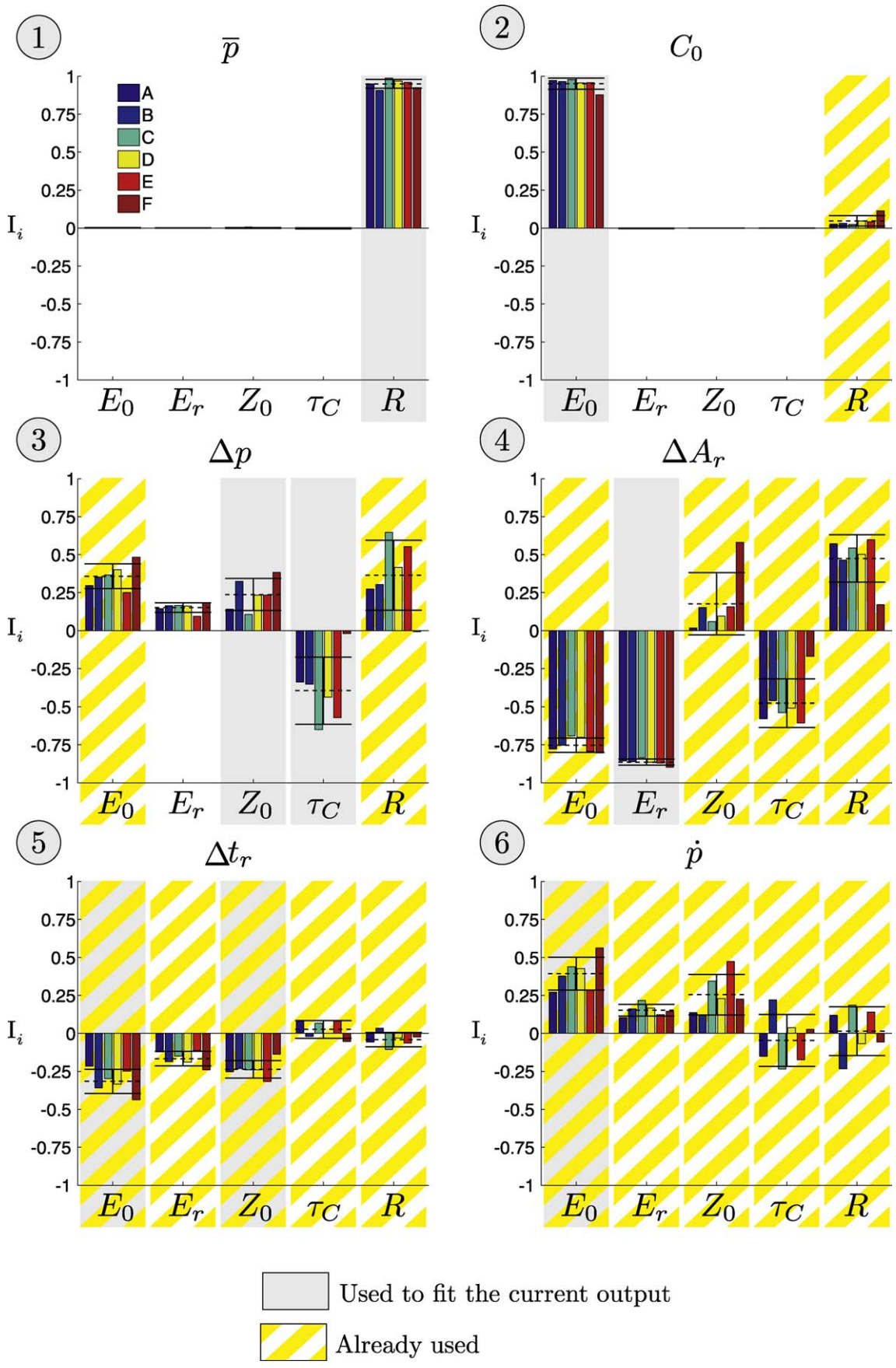

Fig. 6. Sensitivity index $I_{i,k}$ representing the percentage increase of the output parameter for 1% increase in the input parameter for the 6 volunteers, labeled with the letters A, B, C, D, E and F. The consecutive fitting steps are numbered from 1 to 6. The linear relationship between R and P and between C_0 and E_0 exhibit a sensitivity index close to 1.

Table 3
Difference in % between the simulated and measured time average pressure $\bar{p}$, pulse pressure Δp, pressure time derivative $\dot{p}$, compliance C_0, transit time Δt and distension ΔA for the 6 volunteers (A–F). The indices r and u refer to the RA and UA.

	$\bar{p}$	Δp	$\dot{p}$	C_0	Δt_r	Δt_u	ΔA_r	ΔA_u
A	0%	0%	−7%	0%	1%	×	−46%	×
B	0%	−2%	−27%	−55%	−35%	−39%	−15%	+128%
C	0%	0%	−35%	−18%	−31%	−38%	+26%	−50%
D	0%	0%	−28%	−68%	−19%	+20%	+15%	−10%
E	0%	0%	+4%	+16%	−33%	−40%	−23%	−9%
F	0%	0%	5%	−42%	−15%	−8%	28%	−53%

3.4. Results of the fitting

A good fit is obtained between the in vivo measured and simulated BP waveforms at the BA, RA and UA for the 6 volunteers, as illustrated in Fig. 7. The BVF, measured distal in the BA for the volunteers A, B and F, can be approximated well by the simulated BVF; see Fig. 8. The differences between the assessed parameters Δp, $\dot{p}$, C_0, Δt_r, Δt_u, ΔA_r and ΔA_u are displayed in Table 3. A physiologically realistic brachial to radial pulse pressure amplification index of (16 ± 5)% is obtained.

3.5. Patient specific parameter estimation

The estimated Young's moduli range from 1.0 to 6.0 MPa with an average of (3.8 ± 1.7) MPa for the BA and from 1.2 to 7.8 MPa with an average of (4.8 ± 2.2) MPa for the radial artery, see Fig. 5. The obtained values for the model parameters E_0, E_r, K_{Z_0}, τ_C and R are depicted in Table 4. The Young's modulus either remains constant or increases towards the distal part of the model. The time constant τ_C is between 0.5 and 2.2. The characteristic impedance factor K_{Z_0} ranges from 0.5 to 1.0.

4. Discussion

To estimate arterial mechanical properties, different methods, based either on distensibility, pulse wave velocity (PWV) or pressure-velocity loop (PU-loop), have previously been proposed. These methods can be employed to determine the arterial mechanical properties either locally or globally. The aim of this study was to investigate the feasibility of a new method that estimates distributed arterial mechanical properties by means of a reverse method combining a wave propagation model as developed by Bessems et al. [13] with several independent ultrasound and blood pressure measurements.

The in vivo measured radius, distension and distensibility presented in this study are comparable with the ones obtained in other studies [42,44,45]. Regarding the Young's modulus estimates, large differences are observed between the results derived with the distensibility, PWV and PU-loop methods. With a group average of (3.5 ± 1.3) MPa, the results obtained in this study with the distensibility method are comparable to the group average Young's modulus of (3.3 ± 2.4) MPa obtained by Mourad et al. from brachial distensibility for healthy volunteers [43], and the group average of (2.2 ± 1.5) and (1.9 ± 1.5) MPa obtained by Dammers et al. in the BA for healthy men and women, respectively [44]. For the PWV method, the derived Young's modulus ranges from 0.8 to 1.2 MPa corresponding to a PWV of (9.6 ± 0.6) m/s, where McLaughl et al. reported a PWV in the BA of 7.4 m/s with a large inter-subject variability. Employing the PU-loop method, Zambanini et al. obtained a PWV of (7.0 ± 0.6) m/s in the BA [46]. However, in the current study, the same method lead to extraordinary high velocities (up to 35 m/s). Our non-physiological results could be explained by the fact that the BVF and distensibility waveforms were measured with a too large time interval. Furthermore, wall distension waveforms were used instead of blood pressure waveforms. For the initialization of the input parameters only the estimates for the Young's modulus obtained with the distensiblity and the PWV methods were used.

The PWV and PU-loop methods neglect the hemodynamic viscous forces, whereas the arteries of the arm tree have a small diameter and therefore viscous forces in these arteries will be relatively large compare to large arteries like the aorta. Furthermore, the pressure signal is assumed to be reflection free during the systolic period, however in this study, it was found that the pressure reflections coming from the peripheral bed (related to the characteristic impedance Z_0) strongly influence the pressure waveforms, also during systole. When the PWV and PU-loop methods were applied to BP and BVF waveforms obtained from the 1D wave propagation model, large differences were found between the estimated Young's modulus and the Young's modulus used for the simulations (results not shown). This implies that indeed the assumptions behind the PWV and PU-loop method lead to a bias in the estimates. Besides, PWV and PU-loop methods are strongly influenced by measurement errors, see Fig. 5, leading to large uncertainties.

Contrary to previous methods, the reverse method presented in this paper relies on a physiological, one-dimensional wave propagation model, which takes into account hemodynamic viscous forces, pressure wave propagation and reflection phenomena that originate from transitions in arterial stiffness, the presence of bifurcations, arterial lumen tapering and the periphery. Furthermore, several independent ultrasound measurements of vessel wall distension and blood flow velocity as well as systolic and diastolic blood pressure measurements are included, which might reduce the sensitivity to measurement errors. The method proposed in this study estimates the distributed arterial properties along each arterial segment, from the BA to the RA, see Fig. 5.

A fitting procedure based on local sensitivity indexes has been developed. A good match was obtained between the in vivo measured and the simulated blood pressure and blood volume flow waveforms at the BA, RA and UA for the 6 volunteers involved in the study. For volunteers A, B and F, the measured BVF waveforms at an intermediate position in the brachial artery are in agreement with the simulated waveforms. The small quantitative differences between the simulated and measured waveforms result from the fact that these measurements were not used for the fitting procedure. The estimated Young's modulus for the brachial artery ranges from 1.0 to 6.0 MPa with an average of (3.8 ± 1.7) MPa. These results are close to the Young's modulus obtained with the distensibility method ((3.5 ± 1.3) MPa) and the results obtained by Mourad et al. [43]. The obtained brachial to radial pulse amplification of (16 ± 5)% is close to the (12 ± 11)% calculated by Verbeke et al. [29]. These results demonstrate the physiological pertinence of the results given by our patient specific model. In 2009, Reymond et al. [15] have shown that a one-dimensional wave propagation model is suitable for accurate reproduction of measured blood pressure and blood volume flow (BVF) waveforms for the complete arterial tree (including the heart) with non-linear visco-elastic arterial wall

Table 4
Final estimates of the Young's modulus in the brachial and radial artery E_b and E_r, respectively, the characteristic impedance factor K_{Z_0}, the time constant τ_C and the total resistance R.

	E_b [MPa]	E_r [MPa]	K_{Z_0}	τ_c [s]	R [GPa s/(m^3)]
A	4.5	0.5	0.6	13	
B	4.0	5.4	1.0	0.5	9
C	6.0	6.0	0.85	0.8	30
D	3.0	3.6	0.9	1.4	45
E	4.0	7.8	0.8	1.0	54
F	1.0	1.2	0.5	2.2	11

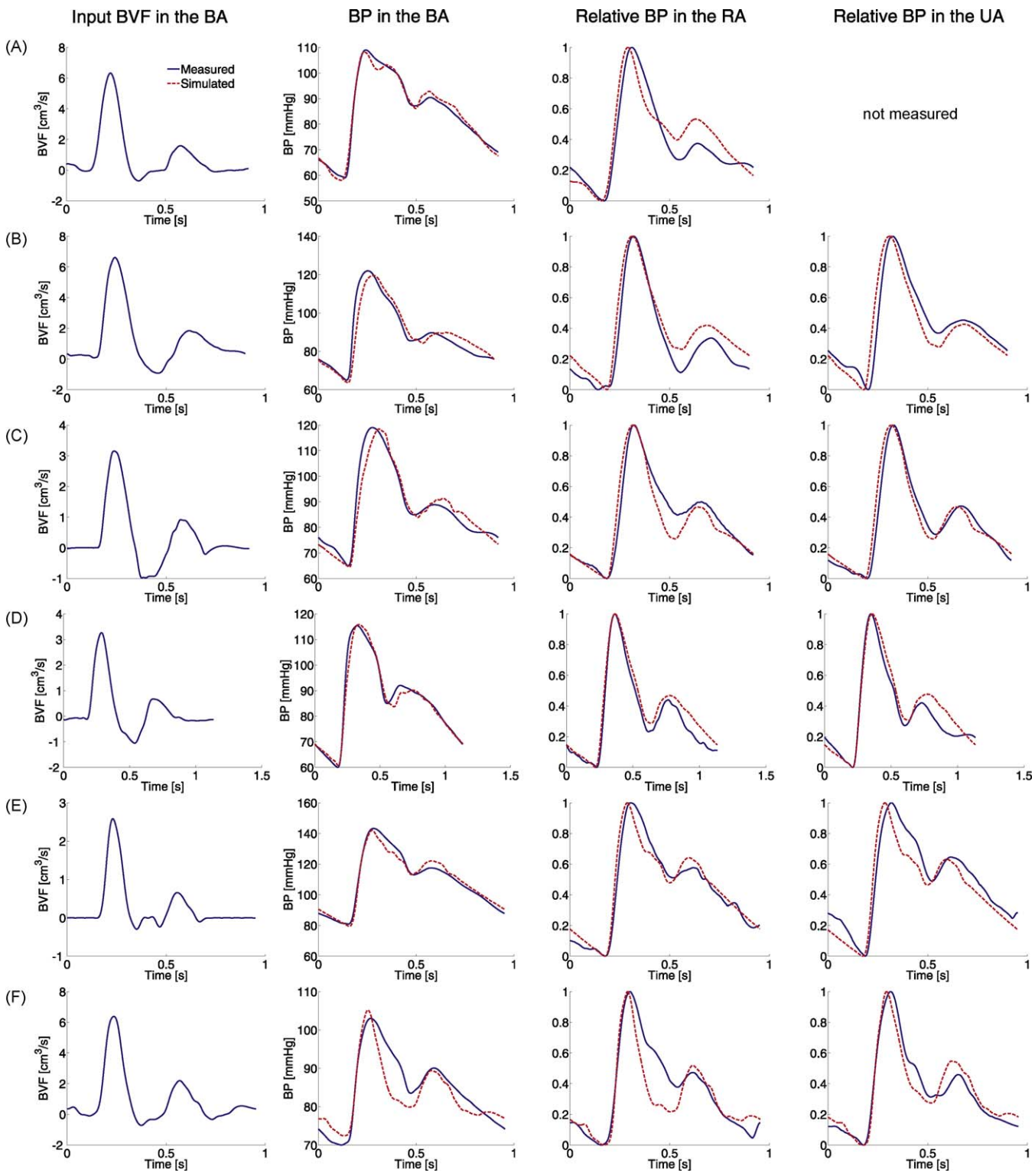

Fig. 7. For each volunteer, labeled with the letters A, B, C, D, E and F, this figure depicts in the 1st column the input blood volume flow (BVF); in the 2nd column the simulated blood pressure (BP) and measured distension waveforms (scaled with P_s and P_d) in the brachial artery (BA); in the 3rd and 4th columns the relative simulated blood pressure and relative measured distension waveforms in the radial (RA) and ulnar (UA) arteries.

properties. Hence, we do expect that the reverse method, as presented in the current study, could be extended to the global arterial tree, and/or more complex arterial properties.

It has been reported that the arterial walls present viscous [47–51] and non-linear behavior [52] whereas in this study an incremental linear elastic model is chosen. Inclusion of viscous properties is very well possible but would imply additional input parameters [53]. Because these parameters cannot easily be assessed in vivo, input uncertainties will then be added and the complexity of the fitting process would increase. Furthermore, the effect of visco-elastic properties is believed to be small for large arteries [50,51]. At high pressures the arterial wall significantly stiffens as elastin fibers are stretched completely [54], and the role of collagen fibers becomes increasingly important. However, under

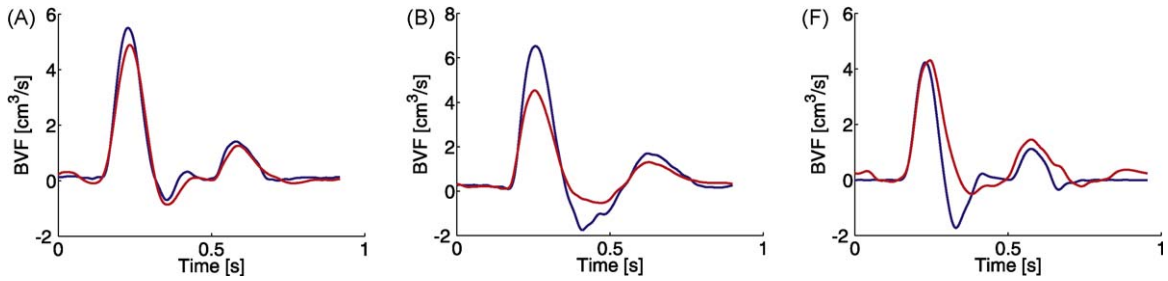

Fig. 8. For volunteers A, B and F this figure depicts in the 1st column: the input blood volume flow (BVF); in the 2nd column: the simulated and measured BVF at an intermediate position in the brachial artery.

normal physiological conditions, the elastin fibers mainly carry the load and non-linearities in mechanical behavior are less significant an linearization by means of an incremental linear model is assumed to be allowed. Consequently, for the present study the viscous and non-linear properties of the arterial wall are ignored.

The measurements used in this study are constrained to large uncertainties, especially for small sized arteries like the radial and ulnar arteries. These uncertainties play a role in the initialization of the input parameters and in the fitting procedure, which uses measured data to fit the simulation results. As a result large differences between the measured and simulated parameters remain, see Table 3. Therefore, in vivo applicability will highly depend on better performance of the ultrasound registration methods.

The reverse method presented in this paper is based on several ultrasound measurements implying a long measurement session that is followed by a complex fitting procedure using a wave propagation model. The method would benefit from simultaneous measurements of the wall distension and blood flow velocity, which would lead to more accurate measurements but also reduce the measurement session duration. Moreover, a global sensitivity analysis [55] could be applied to identify the input parameters that influence the output most. The measurement session duration could be reduced if the focus is on the measurements deserving the most attention.

The diameters sparsely measured along the arterial tree were interpolated using an exponential decay of the area [10,26,37] and Murray's law at the bifurcations [38,39]. Unfortunately, it was not possible to compare the derived geometry to a patient specific geometry. Magnetic resonance imaging might be employed to determine arterial segment lengths for those parts the current spatial resolution allows accurate estimation of the arterial diameter [56].

The local sensitivity analysis demonstrates a complex relationship between the model parameters and the simulated pressure and BVF waveforms. It is thus difficult to find the unique parameter set that corresponds to the absolute best fit between measured and simulated parameters. A global sensitivity analysis [55] or parametric uncertainty analysis [57] could help to understand the model's response to changes in input parameters in a wide range. The results of such a study could improve the fitting procedure towards a more automatic approach utilizing optimization algorithms [58]. For example, Masson et al. employed nonlinear Levenberg-Marquardt least squares minimization to identify local arterial wall properties [59] while Liauh et al. used the adjoint method [60,61] for hyperthermia problems during cancer treatment [62]. Unfortunately, optimization methods require a large number of simulations. To apply such methods to the presented wave propagation model, large computational facilities like grids are necessary to keep the simulation time realistic [63].

In summary, a reverse method to estimate distributed arterial mechanical properties has been presented. This reverse method uses several ultrasound measurements as well as a wave propagation model. A fitting procedure, based on local sensitivity indices, has been developed. A good match has been obtained between the in vivo measured and simulated blood pressure and BVF waveforms.

Conflict of interest

There are no conflicts of interest.

Acknowledgments

This research was supported by a Marie Curie Early Stage Research Training Fellowship of the European Community's Sixth Framework Programme under contact number MEST-CT-2004-514421.

References

[1] Laurent S, Cockcroft J, van Bortel L, Boutouyrie P, Giannattasio C, Hayoz D, et al. Expert consensus document on arterial stiffness: methodological issues and clinical applications. Eur Heart J 2006;27:2588–605.
[2] Blacher J, Pannier B, Guerin A, Marchais S, Safar M, London G. Carotid arterial stiffness as a predictor of cardiovascular and all-cause mortality in end-stage renal disease. Hypertension 1998;32:570–4.
[3] Germain D, Boutouyrie P, Laloux B, Laurent S. Arterial remodeling and stiffness in patients with pseudoxanthoma elasticum. Arterioscler Thromb Vasc Biol 2003;23:836–41.
[4] Guerin A, London G, Marchais S, Metivier F. Arterial stiffening and vascular calcifications in end-stage renal disease. Nephrol Dial Transplant 2000;15:1014–21.
[5] Mattace-Raso F, van der Cammen T, Hofman A, van Popele N, Bos M, Schalekamp M, et al. Arterial stiffness and risk of coronary heart disease and stroke: the rotterdam study. Circulation 2006;113:657–63.
[6] Yufu K, Takahashi N, Anan F, Hara M, Yoshimatsu H, Saikawa T. Brachial arterial stiffness predicts coronary atherosclerosis in patients at risk for cardiovascular diseases. Jpn Heart J 2004;45:231–42.
[7] Avolio A. Multi-branched model of the human arterial system. Med Biol Eng Comput 1980;18:709–18.
[8] Lanzarone E, Liani P, Baselli G, Costantino M. Model of arterial tree and peripheral control for the study of physiological and assisted circulation. Med Eng Phys 2007;29:542–55.
[9] Liang F, Liu H. A closed-loop lumped parameter computational model for human cardiovascular system. JSME Int Ser C 2005;48:484–93.
[10] Olufsen M, Peskin C, Kim W, Pedersen E, Nadim A, Larsen J. Numerical simulation and experimental validation of blood flow in arteries with structured-tree outflow conditions. Ann Biomed Eng 2000;28:1281–99.
[11] Westerhof N, Bosman F, Vries C, Noordergraaf A. Analog studies of the human systemic arterial tree. J Biomech 1969;2:121–43.
[12] Azer K, Peskin C. A one-dimensional model of blood flow in arteries with friction and convection based on the womersley velocity profile. Cardiovasc Eng 2007;7:51–73.
[13] Bessems D, Rutten M, van de Vosse F. A wave propagation model of blood flow in large vessels using an approximate velocity profile function. J Fluid Mech 2007;580:145–68.
[14] Formaggia L, Lamponi D, Tuveri M, Veneziani A. Numerical modeling of 1d arterial networks coupled with a lumped parameters description of the heart. Comput Methods Biomech Biomed Eng 2006;9:273–88.
[15] Reymond P, Merenda F, Perren F, Rüfenacht D, Stergiopulos N. Validation of a one-dimensional model of the systemic arterial tree. Am J Physiol Heart Circ Physiol 2009;297:H208–22.
[16] Sherwin S, Franke V, Peiró J, Parker K. One-dimensional modelling of a vascular network in space-time variables. J Eng Math 2003;47:217–50.

[17] Matthys K, Alastruey J, Peiró J, Khir A, Segers P, Verdonck P, et al. Pulse wave propagation in a model human arterial network: assessment of 1-d numerical simulations against in vitro measurements. J Biomech 2007;40:3476–86.
[18] Bessems D, Giannopapa C, Rutten M, van de Vosse F. Experimental validation of a time-domain-based wave propagation model of blood flow in viscoelastic vessels. J Biomech 2008;41:284–91.
[19] Marchandise E, Willemet M, Lacroix V. A numerical hemodynamic tool for predictive vascular surgery. Med Eng Phys 2009;31:131–44.
[20] Leguy C, Bosboom E, Hoeks A, van de Vosse F. Model-based assessment of dynamic arterial blood volume flow from ultrasound measurements. Med Biol Eng Comput 2009;47:641–8.
[21] Henry R, Kostense P, Spijkerman A, Dekker J, Nijpels G, Heine R, et al. Arterial stiffness increases with deteriorating glucose tolerance status: the Hoorn study. Circulation 2003;107:2089–95.
[22] Smilde T, van den Berkmortel F, Boers G, Wollersheim H, de Boo T, van Langen H, et al. Carotid and femoral artery wall thickness and stiffness in patients at risk for cardiovascular disease, with special emphasis on hyperhomocysteinemia. Arterioscler Thromb Vasc Biol 1998;18:1958–63.
[23] Hermeling E, Reesink K, Kornmann L, Reneman R, Hoeks A. The dicrotic notch as alternative time-reference point to measure local pulse wave velocity in the carotid artery by means of ultrasonography. J Hypertens 2009;27:2028–35.
[24] Parker K, Jones C. Forward and backward running waves in the arteries: analysis using the method of characteristics. J Biomech Eng 1990;112:322–6.
[25] Vermeersch S, Rietzschel E, Buyzere M, Bacquer D, Backer G, van Bortel L, et al. Determining carotid artery pressure from scaled diameter waveforms: comparison and validation of calibration techniques in 2026 subjects. Physiol Meas 2008;29:1267–80.
[26] Anliker M, Rockwell R, Ogden E. Nonlinear analysis of flow pulses and shock waves in arteries. Z Angew Math Phys 1971;22:563–81.
[27] Michel E, Zernikow B. Gosling's Doppler pulsatility index revisited. Ultrasound Med Biol 1998;24:597–9.
[28] Stroev P, Hoskins P, Easson W. Distribution of wall shear rate throughout the arterial tree: a case study. Atherosclerosis 2007;191:276–80.
[29] Verbeke F, Segers P, Heireman S, Vanholder R, Verdonck P, van Bortel L. Noninvasive assessment of local pulse pressure: importance of brachial-to-radial pressure amplification. Hypertension 2005;46:244–8.
[30] Samijo S, Willigers J, Brands P, Barkhuysen R, Reneman R, Kitslaar P, et al. Reproducibility of shear rate and shear stress assessment by means of ultrasound in the common carotid artery of young human males and females. Ultrasound Med Biol 1997;23:583–90.
[31] Brands P, Hoeks A, Willigers J, Willekes C, Reneman R. An integrated system for the non-invasive assessment of vessel wall and hemodynamic properties of large arteries by means of ultrasound. Eur J Ultrasound 1999;9:257–66.
[32] Brands P, Hoeks A, Hofstra L, Reneman R. A noninvasive method to estimate wall shear rate using ultrasound. Ultrasound Med Biol 1995;21:171–85.
[33] Ledoux L, Brands P, Hoeks A. Reduction of the clutter component in doppler ultrasound signals based on singular value decomposition: a simulation study. Ultrason Imaging 1997;19:1–18.
[34] Hoeks AP, Hennerici M, Reneman R. Spectral composition of Doppler signals. Ultrasound Med Biol 1991;17:751–60.
[35] Womersley J. Mathematical theory of oscillating flow in an elastic tube. J Physiol 1955;127, 37–8P.
[36] Stergiopulos N, Segers P, Westerhof N. Use of pulse pressure method for estimating total arterial compliance in vivo. Am J Physiol 1999;276:H424–8.
[37] Fung Y. Biomechanics: circulation. Berlin: Springer; 1996.
[38] Murray C. The physiological principle of minimum work. I. The vascular system and the cost of blood volume. Proc Natl Acad Sci USA 1926;12:207–14.
[39] Painter P, Edén P, Bengtsson H. Pulsatile blood flow, shear force, energy dissipation and murray's law. Theor Biol Med Model 2006;31:3–31.
[40] Benard N, Perrault R, Coisne D. Computational approach to estimating the effects of blood properties on changes in intra-stent flow. Ann Biomed Eng 2006;34:1259–71.
[41] Kaiser D, Mullen K, Bank A. Brachial artery elastic mechanics in patients with heart failure. Hypertension 2001;38:1440–5.
[42] Ku Y, Kim Y, Kim J, Choi Y, Yoon S, Kim Y, et al. Ultrasonographic measurement of intima-media thickness of radial artery in pre-dialysis uraemic patients: comparison with histological examination. Nephrol Dial Transplant 2006;21:715–20.
[43] Mourad J, Girerd X, Boutouyrie P, Laurent S, Safar M, London G. Increased stiffness of radial artery wall material in end-stage renal disease. Hypertension 1997;30:1425–30.
[44] Dammers R, Tordoir J, Hameleers J, Kitslaar P, Hoeks A. Brachial artery shear stress is independent of gender or age and does not modify vessel wall mechanical properties. Ultrasound Med Biol 2002;28:1015–22.
[45] van der Heijden-Spek J, Staessen J, Fagard R, Hoeks A, Boudier H, van Bortel L. Effect of age on brachial artery wall properties differs from the aorta and is gender dependent: a population study. Hypertension 2000;35:637–42.
[46] Zambanini A, Cunningham S, Parker K, Khir A, Thom S, Hughes A. Wave-energy patterns in carotid, brachial, and radial arteries: a noninvasive approach using wave-intensity analysis. Am J Physiol Heart Circ Physiol 2005;289:H270–6.
[47] Learoyd B, Taylor M. Alterations with age in the viscoelastic properties of human arterial walls. Circ Res 1966;18:278–92.
[48] Boutouyrie P, Bézie Y, Lacolley P, Challande P, Chamiot-Clerc P, Benetos A, et al. In vivo/in vitro comparison of rat abdominal aorta wall viscosity. Influence of endothelial function. Arterioscler Thromb Vasc Biol 1997;17:1346–55.
[49] Gow B, Taylor M. Measurement of viscoelastic properties of arteries in the living dog. Circ Res 1968;23:111–22.
[50] Armentano R, Barra J, Levenson J, Simon A, Pichel R. Arterial wall mechanics in conscious dogs. Assessment of viscous, inertial, and elastic moduli to characterize aortic wall behavior. Circ Res 1995;76:468–78.
[51] Gamero L, Armentano R, Barra J, Simon A, Levenson J. Identification of arterial wall dynamics in conscious dogs. Exp Physiol 2001;86:519–28.
[52] Bank A, Kaiser D, Rajala S, Cheng A. In vivo human brachial artery elastic mechanics: effects of smooth muscle relaxation. Circulation 1999;100:41–7.
[53] Tsamis A, Stergiopulos N. Arterial remodeling in response to hypertension using a constituent-based model. Am J Physiol Heart Circ Physiol 2007;293:H3130–9.
[54] Fonck E, Prod'hom G, Roy S, Augsburger L, Rüfenacht DA, Stergiopulos N. Effect of elastin degradation on carotid wall mechanics as assessed by a constituent-based biomechanical model. Am J Physiol Heart Circ Physiol 2007;292:H2754–63.
[55] Saltelli A, Ratto M, Andres T, Campolongo F, Cariboni J, Gatelli D, et al. Global sensitivity analysis: the primer. Wiley; 2008.
[56] Hoogeveen R, Bakker C, Viergever M. Limits to the accuracy of vessel diameter measurement in MR angiography. J Magn Reson Imaging 1998;8:1228–35.
[57] Xiu D, Sherwin S. Parametric uncertainty analysis of pulse wave propagation in a model of a human arterial network. J Comput Phys 2007;226:1385–407.
[58] Antoniou A, Lu W-S. Practical optimization. Springer; 2007.
[59] Masson I, Boutouyrie P, Laurent S, Humphrey J, Zidi M. Characterization of arterial wall mechanical behavior and stresses from human clinical data. J Biomech 2008;41:2618–27.
[60] Jacquard P, Jain C. Permeability distribution from field pressure data. Soc Petrol Eng J 1965;5:281–94.
[61] Carter R, Kemp L, Pearce A, Williams D. Performance matching with constraints. Soc Petrol Eng J 1974;14:187–96.
[62] Liauh C, Hills R, Roemer R. Comparison of the adjoint and influence coefficient methods for solving the inverse hyperthermia problem. J Biomech Eng 1993;115:63–71.
[63] Su A, Berman F, Wolski R, Strout M. Using AppLeS to schedule simple SARA on the computational grid. Int J High Perform Comput Appl 1999;13:253–62.